0.43 THz emission from high-T_c superconducting emitters optimized at 77 K

H Minami[1,2], C Watanabe[1], T Kashiwagi[1,2], T Yamamoto[3], K Kadowaki[1,2], and R A Klemm[4]

[1]Graduate School of Pure and Applied Sciences, University of Tsukuba, 1-1-1 Tennodai, Tsukuba, Ibaraki 305-8573, Japan
[2]Division of Materials Science, Faculty of Pure and Applied Sciences, University of Tsukuba, 1-1-1 Tennodai, Tsukuba, Ibaraki 305-8573, Japan
[3]Institute for Quantum Optics and Center for Integrated Quantum Science and Technology Ulm University, Ulm D-89081, Germany
[4]Department of Physics, University of Central Florida, Orlando, Florida 32816-2385 USA

E-mail: minami@bk.tsukuba.ac.jp

Abstract. A liquid helium-free, compact and continuous sub-terahertz radiation system operating at 77 K has been developed using a rectangular mesa device made from a high T_c-superconducting $Bi_2Sr_2CaCu_2O_{8+\delta}$ single crystal, based on a different design of a stand-alone mesa sandwich structure to reduce the *dc*-current Joule heating effects. The mesa was thermally connected to sapphire plates through thin thermal grease embedded with diamond nano-crystals. When immersed in liquid N_2, the device emits intense radiation at 0.437 THz, the highest frequency ever achieved at 77 K, due to excitation of the TM(1,0) rectangular cavity mode. By varying the *dc* current-voltage bias and the bath temperature in a He-flow cryostat, the device's emission frequency is broadly tunable from 0.31 THz at 79 K to 1.31 THz at 30 K.

PACS numbers: 85.25.Cp

1. Introduction

Electronic devices generating monochromatic electromagnetic (EM) waves in general encounter severe difficulties as their emission frequency f increases to the terahertz (THz, 10^{12} c/s) region and above, because they utilize increasing high-speed carrier velocities in devices with decreasing response times. Correspondingly, the generation of EM waves from photonic devices utilizes photons emitted through electronic energy level transitions $\Delta E = hf$, where h is Planck's constant, which becomes increasingly difficult as f decreases, due to thermal broadening of the energy levels, *etc.* Even with the present electronic and optical technologies, compact and all-solid-state emitting devices that operate successfully in the central portion of the THz band, especially the region between 1 and 2 THz, often denoted the "*THz gap*" [1, 2], have been very difficult to obtain. Among the various approaches to filling the THz gap, quantum-cascade lasers (QCLs) [3] and resonant tunneling diodes (RTDs) [4] have been considered to be the most feasible compact emitters. Continuous-wave QCLs have recently expanded the frequency range down to 1.2 THz with the power of 0.12 mW at 10 K in zero magnetic field [5]. They can generate high power even at such low frequencies, but work only below a critical temperature $T_{\max}$. In general, thermal broadening causes a QCL's emission power to decrease with increasing temperature T, until its lasing action stops working for $T > T_{\max}$, where $T_{\max}(\mathrm{K}) = (h/k_{\mathrm{B}})f \approx 50f$ (THz) [6] and k_{B} is Boltzmann's constant. Hence, QCLs can only be used for $f < 2$ THz by cooling them to $T < 100$ K. On the other hand, RTDs have the great advantage of working at room temperature, and RTD arrays recently attained the emission power of 610 μW at 0.62 THz [7]. The f range has been further extended up to 1.42 THz, but the output power is ~ 1 μW [8].

In 2007, a sub-THz emitting device made from a high transition temperature T_{c} superconductor $Bi_2Sr_2CaCu_2O_{8+\delta}$ (BSCCO) single crystal with $T_{\mathrm{c}} = 90$ K was first reported [9, 10]. This unique device was found to emit continuous, monochromatic, and coherent sub-THz EM waves, which may eventually completely fill the THz gap, because at optimal oxygen doping, the large superconducting energy gap $2\Delta(T = 0) \approx 60$ meV only restricts f to $f \lesssim 2\Delta(T)/h \approx 15$ THz for T not too close to T_{c}, where 1.0 THz corresponds to 4.1 meV. The emission mechanism is attributed to the resonant synchronization of the stack of $N \sim 10^3$ equivalent intrinsic Josephson junctions (IJJs) in a single crystal BSCCO mesa structure, with f matching an appropriate cavity resonance frequency. Since the BSCCO single crystal is composed of a stack of the many superconducting CuO_2 double layers separated by ~ 1.2 nm of insulating Bi-Sr-O layers, it behaves as a series-connected periodic array of IJJs, each 1.533 nm thick [11]. Each intrinsic Josephson junction works as a *dc*-voltage to high-frequency *ac*-current converter, according to the *ac*-Josephson effect, for which f satisfies $f = f_{\mathrm{J}} = (2e/h)V/N$, where e is the electronic charge and V is the *dc* voltage applied across the mesa. Applying 1 mV per junction corresponds to 0.483597870(11) THz [12]. They are so densely packed within a mesa that the *ac* currents across each of the junctions synchronize to produce macroscopic coherent current oscillations, thereby

generating coherently intensified sub-terahertz emission [13, 14]. This synchronization is enhanced by the geometrical cavity resonance condition, $f = f_c(m, p)$, where m and p are integral mode indices for the particular thin geometrical cavity shape. For a thin rectangular mesa of width w and length ℓ, $f_c(m, p) = \frac{c_0}{2n}\sqrt{(m/w)^2 + (p/\ell)^2}$ [15, 16], where $n \approx 4.2$ is the index of refraction for BSCCO and c_0 is the speed of light in vacuum. For long rectangular mesas, the emission frequencies are usually inversely proportional to w[9, 17, 18]. Since the emission power $P \propto N_{\rm act}^2$, where $N_{\rm act}$ is the number of active Josephson junctions [9], *i.e.*, corresponding to the effective thickness of the rectangular mesa, a few tens of μW can be obtained in the (sub-)THz frequency region [18, 19, 20, 21, 22, 23].

When the IJJ emitter is in its voltage state, a serious problem has arisen from severe Joule heating ($\sim$ 1 MW/cm^3) due to the injected *dc*-current I into the mesa. Below about 50 K, this self heating occurs very locally, due mainly to the poor BSCCO thermal conductivity at low T and to the strongly negative temperature derivative of the c-axis resistivity, and forms a spot-like normal conducting region with the local temperature $T(\boldsymbol{r}) > T_{\rm c}$, known as a "*hot spot*" [24, 25, 26, 27, 28]. Since the hot spot short circuits the *dc*-bias current flow, it behaves as a shunt resistor [29]. In previous studies the severe self heating and hot-spot formation were revealed to suppress the upper limits of the operation temperature and the frequency, and also to decrease the emission power significantly [19, 21]. Moreover, the interference of the heating between mesas made it difficult for mesa arrays to emit coherently [30].

The Joule heating problem can be alleviated by making better thermal connections between the mesa and thermal bath. "*Stand-alone*" mesa devices, with a direct metallic connection of the mesa surface to the bath, were first suggested [15, 16] and then fabricated and studied [18, 20, 21, 22, 31]. In addition, a modified stand-alone mesa device obtained by removing part of the BSCCO superconducting base and making the remaining part and the polyimide glue between the mesa and the sapphire substrate sufficiently thin was also investigated [19]. These structures greatly improved the thermal contact between the mesa and the thermal bath, as demonstrated by the facts that the maximum operation bath temperature $T_{\rm b}$ was increased to above 70 K and the maximum emission intensity was observed around 55 K [19, 21], at and above which the earlier mesas had stopped emitting [17]. The emission frequencies were also increased, with $f \sim 1.05$ THz observed at $T_{\rm b} = 20$ K by such heat management [21, 31]. Very recently, emission up to 2.4 THz was also observed at $T_{\rm b} = 15$ K in a stand-alone type of mesa, which was cooled from both top and bottom surfaces through a metallic Au contact sandwiched between thick insulating sapphire layers, without any BSCCO superconducting base or polyimide glue [32, 33]. By using a similar sandwiched stand-alone mesa device, Hao *et al.* recently reported that it works over the frequency range from 0.323 THz to 0.364 THz in liquid nitrogen [34].

Here, we report on a THz emitting system operating at $T_{\rm b} = 77$ K in an entirely helium-free micro-cryostat. Although the mesa used in this experiment was a "conventional" one still having the superconducting BSCCO substrate, the device

structure employs a simpler design from that of sandwiched stand-alone mesa structures to alleviate the Joule heating problem. In spite of the simple construction of the present mesa device structure, it provides excellent sub-THz emission performance. At 77 K, a record high $f = 0.437$ THz was obtained, and because the emission was apparently enhanced by its resonance with the rectangular TM (1,0) cavity mode, its intensity was sufficiently strong for its possible utility in applications. Moreover, by varying $T_{\rm b}$ in a He-flow cryostat, the device's emission can be tuned over the wide frequency range from 0.31 THz to 1.31 THz. This simpler heat removal design allows for flexibility and variety in the construction of future devices with improved emission performances.

2. Experimental

A piece of a cleaved single crystal of slightly underdoped BSCCO with $T_{\rm c} = 90$ K and lateral dimensions of a few mm^2 was glued tightly to a sapphire substrate by polyimide. Three rectangular mesas nominally 80 μm in width, 400 μm in length and 2.0 μm in height were fabricated by an Ar-ion milling technique using metal masks, by which it is much easier to make thicker mesas than by the photolithography technique [35]. This intermediate structure is similar to the conventional mesas studied earlier [9, 17]. Details of this preliminary fabrication process were given previously [18].

A top-view photograph of the device is shown in Fig. 1(a). The mesa dimensions measured by an atomic force microscope (Keyence, VN8000/8010) had in fact a trapezoidal cross-sectional shape, with the top and the bottom widths of 79 μm and 89 μm, respectively. The top of this mesa device was covered by a sapphire plate using insulating thermal grease containing diamond nanocrystals, and the entire device was sandwiched between Cu plates with the same grease, as shown in Figs. 1(b) and 1(c), where a photograph of the assembled entire device and a cross-sectional sketch of its structure, respectively, are shown. The Cu plates sandwiching the sapphire plates that respectively sandwich the thermal grease with diamond nanocrystals and the mesa with attached electrical leads are gently pressed by four screws at the corners of the top Cu plate, in order to reduce the Joule heating as much as possible. Unlike previous studies [32, 33, 31, 34, 36], a focusing lens was not used in the present device. When operating at 77 K, the entire device is immersed in liquid nitrogen. The THz radiation was sent by way of a thin CuNi wave guide 3.2 mm in inner diameter and 20 cm in length to a compact Schottky barrier diode (SBD) at the top of the micro-cryostat, as sketched in Fig. 1(c). When the THz device is operated in a He-flow cryostat (down to 4.2 K) or in a liquid nitrogen cryostat (down to 77 K), the device was tightly mounted onto the Cu cold finger base, and the THz radiation was allowed to pass through either a polyethylene or a quartz cryostat window.

The mesa was biased by a *dc* current/voltage source with a load resistor of 10 Ω connected in series for I measurements. The THz radiation was amplitude-modulated by using either an optical chopper at 70 Hz or a bias modulation from 20 to 100 kHz with a rectangular wave superimposed upon the *dc* bias V, and detected by either an

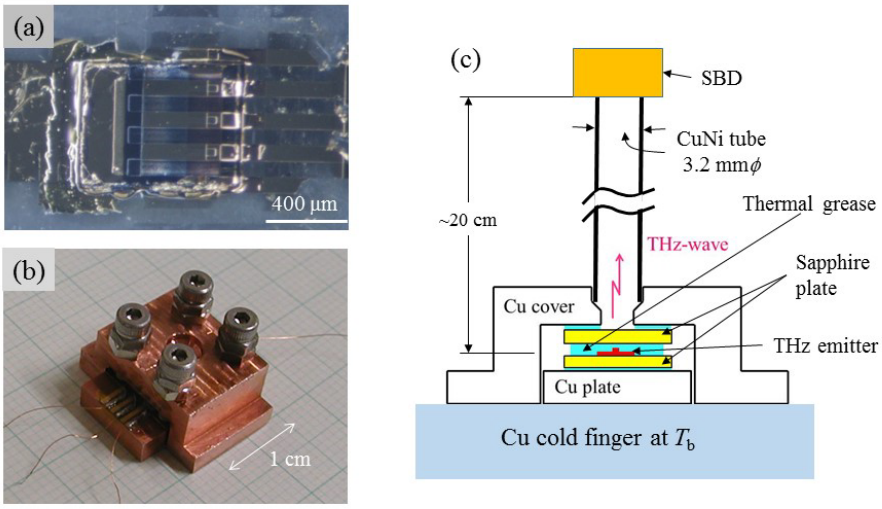

Figure 1. (a) A top-view photograph of the high-T_c superconducting THz emitting device used for the present experiments. Three mesas are shown on the surface of a BSCCO single crystal glued to a sapphire substrate by polyimide glue. The scale is shown at the bottom. (b) A photograph of the entire device sitting on mm-sectioned graph paper. (c) A cross-sectional sketch of the THz emitting device. The superconducting BSCCO mesa is embedded in diamond-containing thermal grease, which is consecutively sandwiched between two sapphire plates and two Cu plates that are gently pressed together with the four corner screws shown in (b).

InSb hot electron bolometer (HEB) at 4.2 K or a SBD attached to a diagonal horn antenna at room temperature. In both cases, the output signals detected were fed to a lock-in amplifier (EG & G 5210) with the time constant of 0.3 s through a low noise preamplifier with a gain of 1,000. The calibrated sensitivity of the HEB (QMC, QFI/2BI) is about 3,300 V/W (without the preamplifier) and its noise equivalent power (NEP) is 0.9 pW/Hz$^{1/2}$. The specified conversion rate of the SBD (VDI, WR1.9ZBD) is about 1,000 V/W (without the preamplifier) between 400 and 600 GHz and its NEP = 4.1 pW/Hz$^{1/2}$. Although the sensitivity of the SBD is lower by an order of magnitude than that of the Si-bolometer, we intentionally used the compact SBD as the detector to integrate it into the small, compact and handy final "*gadget*" containing both the source and the receiver. The radiation spectra were analyzed by a Fourier-transform infrared (FT-IR) spectrometer (JASCO Co., Japan, FARIS-1) with 7.5 GHz resolution, using a Si-composite bolometer as the detector [17].

3. Results and discussion

The I-V characteristics (IVCs) of one of three mesas measured by the two-terminal method using a *dcI* source are presented in Fig. 2(a) for the color-coded T_b from 10 K to 78 K. The data were taken in a He-flow cryostat to compare the characteristics of the present device with those of previous devices obtained under the same experimental conditions. As seen in Fig. 2(a), these IVCs exhibit the large hysteresis and branching structure typical of stacked IJJs [11] even at 78 K. The sharp jump in the bias V for 13 mA $\lesssim I \lesssim$ 22 mA is indicative of the formation of a hot spot in the mesa for $T_\mathrm{b} \leq 50$ K, as observed previously [29]. On the return branch at $T_\mathrm{b} = 10$ K, as highlighted by the black arrows in the upper right and lower left quadrants of Fig. 2(a), the bias V jumps suddenly to its maximum magnitude of 3.83 V at $I = 13.7$ mA. This value is much larger, and the IVC back bending is less pronounced, than those IVC features obtained from conventional mesas with the same thickness. These features suggest that the local temperature $T(\boldsymbol{r})$ rise of the mesa is reduced from that measured directly atop conventional mesas at the same T_b [29], most likely due to the present device's better thermal bath contact. These results show that the heat removal through the thermal nano-diamond grease from the upper surface of the mesa has comparable efficiency to that of stand-alone mesa structures, although the present device uses the conventional mesa structure with the same BSCCO crystal as the superconducting base. Note that the initial critical current $I_\mathrm{c} \sim 110$ mA at $T_\mathrm{b} = 10$ K is several times higher than that used in previous studies, because the single crystal used here was nearly optimally doped, as its $T_\mathrm{c} \sim 90$ K.

The THz emission was detected by a lock-in technique with an amplitude modulation of the radiation power at 70 Hz by the optical chopper set just in front of the HEB detector to which the fraction of the THz radiation present in the solid angle of $\sim 2.0 \times 10^{-2}$ sr was guided after passing through a polyethylene window in the He-flow cryostat. The IVCs were measured simultaneously. Figures 2(b) and 2(c) present the observed voltage output of the HEB detector as functions of the bias V and I, respectively, after subtraction for the constant background arising from room-temperature thermal radiation. The T_b color code in (a) also applies to (b) and (c). The inset (d) to Fig. 2(a) displays plots of the HEB outputs of the strong emissions observed at the biases $V \sim 0.9$ V and 2.2 V versus T_b. The weaker emission for $V \sim 2.2$ V was observed for $T_\mathrm{b} < 60$ K, and is depicted by the broad blue peak in (d). This emission has a maximum HEB output of 4 mV corresponding to 3.3 nW power at 40 K. For T_b below ~ 50 K, the intensity is low, but f is as high as 0.8 THz, corresponding to the TM(2,0) rectangular EM cavity mode. But the surprising feature is the strong emission power versus T_b peak depicted in red and labeled "~ 0.9 V" that was observed at the higher T_b range between 65 and 80 K. This peak has a maximum at 75 K with the HEB output of 18 mV corresponding to the detected power of 15 nW. With increasing T_b, although the IVC hysteresis steadily shrinks, as is usually seen, it is remarkable that THz radiation can still be observed even up to 80 K. f for this high-

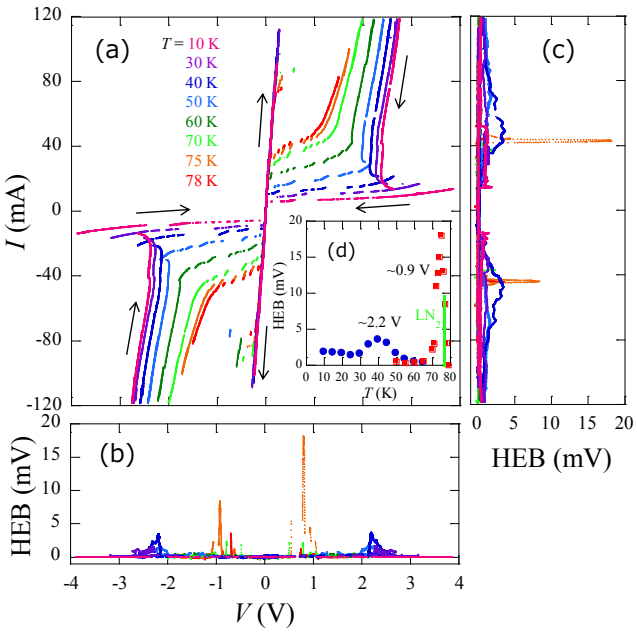

Figure 2. (a) Color-coded T_b dependence from 10 K to 78 K of the IVCs of a BSCCO mesa device cooled by the He-flow cryostat. No corrections for the residual resistance of 2.4 Ω due to Au films, leads, *etc.*, were made in this plot. The arrows indicate the direction of the data acquisition. (b) and (c) The HEB output voltage measured as respective functions of either bias V or I at the T_b values corresponding to the color code in (a) is displayed. (d) The maximum THz emission intensity as a function of T_b is shown. The green vertical line highlights $T_b = 77$ K. The high and low T_b peaks are depicted in red and blue, respectively.

T_b emission is $\sim$ 0.4 THz, which corresponds to the TM(1,0) rectangular EM cavity mode. At $T_b = 78$ K, emission occurs at the bias values $V \sim 0.8$ V and $I \sim 45$ mA and clearly hysteretic IVCs are seen in Fig. 2(a). Remarkably, the emission intensity has its overall maximum at $T_b \sim 75$ K. Although this value depends slightly upon the mesa, it is very different than the optimum intensity T_b range of 30 K to 40 K observed for the earliest mesas[9, 17], and of 50 to 60 K for the more recent mesas which have only a thin superconducting substrate underneath the mesa [19] or for other stand-alone mesa types [21]. Consequently, these results demonstrate that the present mesa device construction provides another effectively excellent heat conduction path, which enables us to generate THz radiation sufficient to construct a compact THz emission and detection system operating even at 77 K.

Figure 3 shows the emission spectra measured at selected T_b values between 30 K and 78 K using another mesa with $T_c = 90$ K, the optimum temperature for maximum emission intensity of which is 72 K. Above 70 K, rather strong sub-THz emission is observed at $\sim$ 0.4 THz with the bias $V \sim 0.9$ V. For $T_b \sim 50$ K, emission is observed at $f \sim 0.8$ THz with the bias $V \sim 2$ V. As T_b is decreased to 30 K, the fundamental

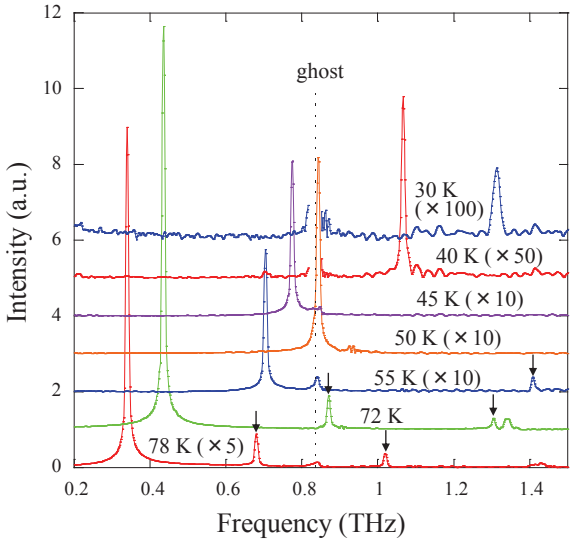

Figure 3. The THz emission spectra measured by a FT-IR spectrometer at the T_b values 30 K, 40 K, 45 K, 50 K, 55 K, 72 K and 78 K. The intensities shown there are respectively multiplied by x=100, 50, 10, 10, 10, 1, 5. The spurious "ghost" peaks present at 0.83 THz in all spectra are due to vibration noise in the Si-bolometer through the helium gas. These spurious peaks were truncated in the 30 K and 40 K spectra. At 55 K, 72 K and 78 K, the higher emission harmonics are indicated by vertical arrows.

peak shifts up to the highest observed $f = 1.31$ THz in this mesa, though its intensity is very weak and the line width is wider than that of others obtained at higher T_b values. The line width of the emission is limited by the instrumental resolution of 7.5 GHz of the FT-IR spectrometer except for the ones obtained at 30 K. In the spectra measured between 55 K and 78 K, the vertical arrows indicate the second and third harmonic emissions, which are clearly observed below 1.5 THz, as seen previously [17].

Figure 4 is a chart that summarizes the emission characteristics of this second sample obtained by measuring its spectral data at many bias points and many T_b values. Overall, the emission was observed over the wide f range from 0.31 to 1.31 THz and T_b range from 30 K to 78 K, as seen in Fig. 4(a). However, the emission intensity strongly depends upon T_b and f, as seen in Figs. 4(b) and 4(c). Note that the strongest emission occurs at $T_b = 72$ K and $f = 0.435$ THz, with the detected power of about 70 nW within the solid angle of $\sim 2.0\times10^{-2}$ sr. Between 69 K and 74 K, the frequencies including that of this strongest emission can be described well by both the *ac*-Josephson relation, $f = f_J$, and the transverse magnetic TM(1,0) cavity resonance mode condition at $f = f_c(1,0)$ corresponding to a half wavelength standing mode across the mesa width, as described above [9, 17, 18]. The trapezoidal cross

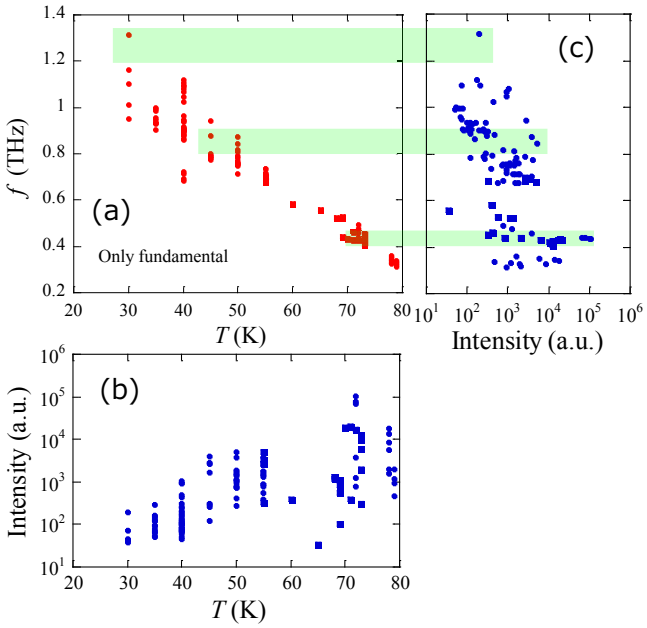

Figure 4. The emission characteristics chart of all of the spectral data taken from many bias points at various T_b values. The emission f and intensity are plotted as functions of T_b in (a) and (b), respectively. The emission intensity is plotted as a function of f in (c). Green bands indicate the predicted TM(n,0) cavity resonances, where $n = 1, 2, 3$.

section of the mesa cavity, with the top and bottom mesa widths 79 μm and $\sim$ 89 μm, respectively, are considered to limit the cavity resonance quality (Q) factor to $\sim$ 10. [10] However, previous measurements showed the emission line widths to be much sharper than expected from this low geometrical Q-factor [18, 37]. This is because of the frequency pulling effect, in which the non-linear collective synchronization of the emission frequencies emitted from each IJJ pulls the emission peaks together, and their combined line width becomes much narrower than that of an individual emission peak alone [10, 37]. The second maximum intensity is seen at $f \sim 0.8$ THz, which corresponds to the cavity TM(2,0) mode at $f = f_c(2, 0)$. The emission at 1.31 THz is within the range of the TM(3,0) mode at $f = f_c(3, 0)$. We only observed weak emission for f in the intermediate regime $\sim$ 0.6 THz, presumably due to the lack of a suitable cavity resonance mode in that regime.

This THz emitting device was then mounted at one end of the hollow CuNi tube wave guide described above, and cooled to 77 K by immersion in liquid nitrogen contained by a small stainless steel dewar. A diagonal horn antenna with the incident area of 4.0 mm^2 was attached to the SBD detector and it was set near the other end of the CuNi tube, which was sealed by a kapton film at the top cryostat flange in order to prevent air condensation, as sketched in Fig. 1(c).

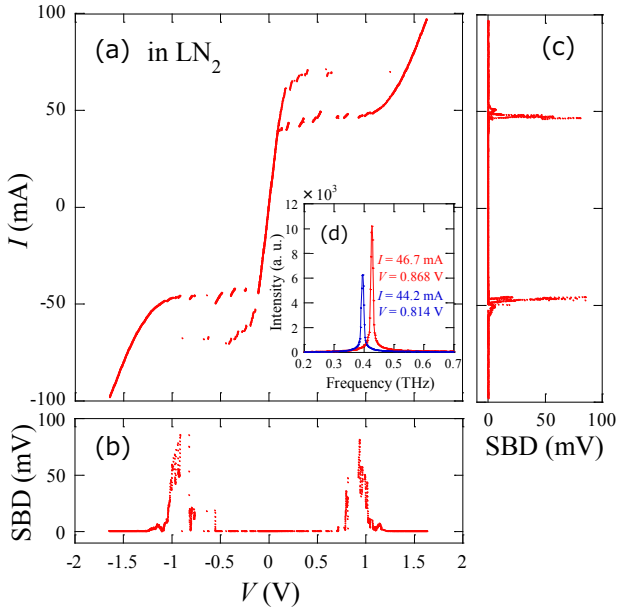

Figure 5. (a) The IVCs of the BSCCO THz emitting mesa device immersed in liquid nitrogen. (b) and (c) The SBD output voltage as functions of bias V and I, respectively. The inset (d) in (a) shows the emission spectra of the BSCCO THz emitting mesa device immersed in liquid nitrogen, measured at two different bias points on the same IVC branch.

Figure 5(a) presents the IVCs of the IJJ emitting device immersed in liquid nitrogen at T_b = 77 K. For THz detection, the full square-wave amplitude modulation was performed by superimposing a 167 mV peak-to-peak *ac* voltage at 73 kHz onto the *dc* bias V. Note that the IVCs shown in Fig. 5(a) are slightly different from those measured with only the *dc* bias (*i. e.*, without the *ac* modulation), as seen for example in Fig. 2(a). However, the differences caused by the *ac* modulation appear at the transitions between branches, but the *ac* modulation does not influence the voltage drops in the high current bias region. The IVCs measured in liquid N_2 shown in Fig. 5(a) appear to be almost exactly the same as those measured at T_b = 73 K or 74 K in the He-flow cryostat, which are close to the sample's optimal emission temperature of 72 K. In fact, as this liquid N_2 emission intensity at T_b = 73 K $\sim$ 74 K is about 80 % of that at the optimal intensity at T_b = 72 K, this THz device can be regarded to be nearly optimized to its maximum emission power while immersed in liquid N_2. Figures 5(b) and 5(c) show the output voltage corresponding to the THz intensity from the SBD detector as functions of bias V and I, respectively. The THz emission is observed at $V \sim 0.85$ V and $I \sim 48$ mA. The terahertz power detected by the SBD detector at the maximum intensity is about 250 nW, while the peak-to-peak noise voltage is 0.15 μV, which corresponds to 150 pW, resulting in the S/N ratio of $\sim 1.7\times10^3$.

Then, the THz radiation from the device immersed in liquid N_2 that emerged from the top end of the CuNi wave guide was deflected 90° from the vertical direction to the appropriate horizontal direction by a flat mirror, then changed to a plane wave form using an off-axial concave mirror before it was finally guided to the FT-IR spectrometer. The mesa was biased only with the *dc* I. The results are shown in inset (d) to Fig. 5(a), where two emissions on the same IVC branch were measured. Their central frequencies are 0.396 THz and 0.427 THz with respective bias points $I = 44.24$ mA, $V = 0.814$ V, and $I = 46.73$ mA, $V = 0.868$ V. Note that the latter frequency is close to that at which the strongest emission was observed using the He-flow cryostat, also suggesting that this device can be considered to be nearly optimized while in liquid N_2. The line widths of the observed spectra are limited by the instrumental resolution of 7.5 GHz of the FT-IR spectrometer. The actual emission frequency can be varied in liquid nitrogen from 0.373 THz to 0.437 THz by varying slightly the bias voltage. It is the highest frequency ever achieved at 77 K from a BSCCO high-T_c superconductor THz emitter, providing evidence that this technique has an excellent heat removal efficiency, comparable to that of the sandwiched stand-alone mesa structures. Furthermore, as clearly seen from Fig. 4, the frequency matches the cavity resonance frequency f_c corresponding to an integer times a half wavelength fundamental standing wave mode $f_c(1,0)$, at which the emission intensity is considerably enhanced. That also suggests that the emission from our device is nearly optimized at liquid nitrogen temperature. We note that in the similar work by Hao *et al.* [34], the radiation frequencies from 0.323 THz to 0.364 THz observed at liquid nitrogen temperature are far from the fundamental cavity resonance frequency range 0.7∼0.8 THz expected for their sample. We finally emphasize that our entire device described above is so simple and compact that it needs no liquid helium tank, transfer tube, He-flow system, vacuum pump, or temperature controller, *etc.* Therefore, the overall sub-THz emitting and detecting system can be easily assembled in approximate dimensions as small as 10 cm × 10 cm × 30 cm and a mass of ∼ 1 kg, using either a liquid nitrogen cryostat or a Stirling refrigerator and the SBD detector.

Considering the advantages and disadvantages of various THz radiation sources, the IJJ THz emitter is unique because its radiation mechanism is entirely different from semiconductor electronic and photonic devices. This radiation mechanism relies purely on the two fundamental principles: one is the *ac*-Josephson effect and the other is the cavity resonance condition of the EM waves. Since the superconducting gap energy 2Δ is potentially as large as 60 meV, if this gap (or its Fermi surface average) were to be isotropic in the *ab* plane for *c*-axis Josephson tunneling processes, one would expect emissions up to 15 THz to be eventually possible from such devices. At present, the observed emissions up to 2.4 THz demonstrate that the lower limit on this gap is at least 9.8 meV[33]. We believe that this advantage, unavailable with other THz sources, overcomes the inevitable disadvantage of low temperature operation requirements below $T_c \sim 90$ K. The remaining limitation for the superconducting IJJ THz emitter is the radiation intensity, which is perhaps insufficient for many

applications. However, this THz device has great potential for further development, for example, by constructing arrays of mesas to intensify the power [38], which have in fact already been demonstrated[30, 35, 39]. Those authors pointed out that the thermal management is difficult and very important for the synchronization of the array emissions. By incorporating the cooling techniques presented here with stand-alone mesa sandwich structures, for example, issues such as the severe thermal interference between the array mesas can be overcome, allowing for relatively easy synchronized array operation.

4. Conclusion

In conclusion, we have demonstrated that entirely He-free, compact, and easy-to-handle THz IJJ emitters made from the high-T_c superconductor $Bi_2Sr_2CaCu_2O_{8+\delta}$ can be operated at 77 K in liquid nitrogen at sub-THz frequencies around 0.43 THz, by electromagnetic wave detection with a Schottky barrier diode operating at room temperature. In order to overcome the severe Joule heating problem, we adopted a different design from that of stand-alone mesa structures. In our design, the heat was removed from the top of a conventional mesa structure to the thermal bath through insulating thermal grease containing diamond nanocrystals. At 77 K, emission frequencies were observed up to 0.437 THz, the record high value for BSCCO THz emitters, including stand-alone BSCCO mesa sandwich structures. Hence, the heat removal efficiency of the present device is comparable to those of the sandwiched stand-alone mesa structures. This different device design also allows for flexibility and variety in future device construction to improve the emission performance, and especially the radiation power. Our emitter was nearly optimized at 77 K, i.e., as the operating frequency at 77 K matched the fundamental cavity resonance frequency $f_c(1,0)$. Therefore, from a Schottky barrier diode detector operating at room temperature, the observed intensity was as high as $\sim$250 nV, resulting in the substantial S/N ratio of $\sim 1.7 \times 10^3$. Finally, by varying the *dc* current-voltage bias and the bath temperature in a He-flow cryostat, the device's emission frequency is broadly tunable from 0.31 THz at 79 K to 1.31 THz at 30 K.

Acknowledgments

The authors would like to express their sincere thanks to all members of the Kadowaki-Kashiwagi laboratory for their assistance in experiments, and in particular to Dr. W. -K. Kwok, Dr. H. B. Wang, and Dr. U. Welp for fruitful discussions. The authors also thank the staff members of the Central Workshop of the University of Tsukuba for machining support. This work was supported by the Japan Society for the Promotion of Science through respective KAKENHI Grant-in-Aid Numbers 15H01996 and 15K04688 for Scientific Research (A) and (C) and 24654097 for Challenging Exploratory Research.

References

[1] Tonouchi M 2007 *Nature Photon.* **1** 97
[2] Lee M and Wanke M C 2007 *Science* **316** 64
[3] Köhler R, Tredicucci A, Beltram F, Beere H E, Linfield E H, Davies A G, Ritchie D A, Iotti R C and Rossi F 2002 *Nature* **417** 156
[4] Brown E R, Söderström J R, Parker C D, Mahoney L J, Molvar K M and McGill T C 1991 *Appl. Phys. Lett.* **58** 2291
[5] Walther C, Fischer M, Scalari G, Terazzi R, Hoyler N and Faist J 2007 *Appl. Phys. Lett.* **91** 131122
[6] Williams B S 2007 *Nature Photon.* **1** 517
[7] Suzuki S, Shiraishi M, Shibayama H and Asada M 2013 *IEEE J. Sel. Top. Quant. Electron.* **19** 8500108
[8] Kanaya H, Sogabe R, Maekawa T, Suzuki S and Asada M 2014 *J. Infrared Milli. Terahz. Waves* **35** 425
[9] Ozyuzer L, Koshelev A E, Kurter C, Gopalsami N, Li Q, Tachiki M, Kadowaki K, Yamamoto T, Minami H, Yamaguchi H, Tachiki T, Gray K E, Kwok W K and Welp U 2007 *Science* **318** 1291
[10] Welp U, Kadowaki K and Kleiner R 2013 *Nature Photon.* **7** 702
[11] Kleiner R, Steinmeyer F, Kunkel G and Müller P 1992 *Phys. Rev. Lett.* **68** 2394
[12] This value is the fundamental constant known as the Josephson constant K_{J}. The value is taken from the "2010 CODATA recommended values".
[13] Koyama T and Tachiki M 1995 *Solid State Commun.* **96** 367
[14] Tachiki M, Iizuka M, Minami K, Tejima S and Nakamura H 2005 *Phys. Rev. B* **71** 134515
[15] Klemm R A and Kadowaki K 2010 *J. Supercond. Nov. Magn.* **23** 613
[16] Klemm R A and Kadowaki K 2010 *J. Phys. Condens. Matter* **22** 375701
[17] Kadowaki K, Yamaguchi H, Kawamata K, Yamamoto T, Minami H, Kakeya I, Welp U, Ozyuzer L, Koshelev A E, Kurter C, Gray K E and Kwok W K 2008 *Physica C* **468** 634
[18] Kashiwagi T, Tsujimoto M, Yamamoto T, Minami H, Yamaki K, Delfanazari K, Deguchi K, Orita N, Koike T, Nakayama R, Kitamura T, Sawamura M, Hagino S, Ishida K, Ivanovic K, Asai H, Tachiki M, Klemm R A and Kadowaki K 2012 *Jpn. J. Appl. Phys.* **51** 010113
[19] Sekimoto S, Watanabe C, Minami H, Yamamoto T, Kashiwagi T, Klemm R A and Kadowaki K 2013 *Appl. Phys. Lett.* **103** 182601
[20] Kadowaki K, Tsujimoto M, Delfanazari K, Kitamura T, Sawamura M, Asai H, Yamamoto T, Ishida K, Watanabe C, Sekimoto S, Nakade K, Yasui Y, Asanuma K, Kashiwagi T, Minami H, Tachiki M, Hattori T and Klemm R A 2013 *Physica C* **491** 2
[21] Kitamura T, Kashiwagi T, Yamamoto T, Tsujimoto M, Watanabe C, Ishida K, Sekimoto S, Asanuma K, Yasui T, Nakade K, Shibano Y, Saiwai Y, Minami H, Klemm R A and Kadowaki K 2014 *Appl. Phys. Lett.* **105** 202603
[22] An D Y, Yuan J, Kinev N, Li M Y, Huang Y, Ji M, Zhang H, Sun Z L, Kang L, Jin B B, Chen J, Li J, Gross B, Ishii A, Hirata K, Hatano T, Koshelets V P, Koelle D, Kleiner R, Wang H B, Xu W W and Wu P H 2013 *Appl. Phys. Lett.* **102** 092601
[23] Turkoglu F, Koseoglu H, Demirhan Y, Ozyuzer L, Preu S, Malzer S, Simsek Y, Muller P, Yamamoto T and Kadowaki K 2012 *Supercond. Sci. Technol.* **25** 125004
[24] Wang H B, Guénon S, Yuan J, Iishi A, Arisawa S, Hatano T, Yamashita T, Koelle D and Kleiner R 2009 *Phys. Rev. Lett.* **102** 017006
[25] Wang H B, Guénon S, Gross B, Yuan J, Jiang Z G, Grünzweig M, Ishii A, Wu P H, Hatano T, Koelle D and Kleiner R 2010 *Phys. Rev. Lett.* **105** 057002
[26] Guénon S, Grünzweig M, Gross B, Yuan J, Jiang Z G, Zhong Y Y, Li M Y, Ishii A, Wu P H, Hatano T, Mints R G, Goldobin E, Koelle D, Wang H B and Kleiner R 2010 *Phys. Rev. B* **82** 214506
[27] Gross B, Guénon S, Yuan J, Li M Y, Li J, Ishii A, Mints R G, Hatano T, Wu P H, Koelle D, Wang H B and Kleiner R 2012 *Phys. Rev. B* **86** 094524

[28] Minami H, Watanabe C, Sato K, Sekimoto S, Yamamoto T, Kashiwagi T, Klemm R A and Kadowaki K 2014 *Phys. Rev. B* **89** 054503
[29] Watanabe C, Minami H, Yamamoto T, Kashiwagi T, Klemm R A and Kadowaki K 2014 *J. Phys. Condens. Matter* **26** 172201
[30] Benseman T M, Gray K E, Koshelev A E, Kwok W K, Welp U, Minami H, Kadowaki K and Yamamoto T 2013 *Appl. Phys. Lett.* **103** 022602
[31] Ji M, Yuan J, Gross B, Rudau F, An D Y, Li M Y, Zhou X J, Huang Y, Sun H C, Zhu Q, Li J, Kinev N, Hatano T, Koshelets V P, Koelle D, Kleiner R, Xu W W, Jin B B, Wang H B, and Wu P H 2014 *Appl. Phys. Lett.* **105** 122602
[32] Kashiwagi T, Yamamoto T, Kitamura T, Asanuma K, Watanabe C, Nakade K, Yasui T, Saiwai Y, Shibano Y, Minami H, Tsujimoto M, Yoshizaki R, Delfanazari K, Klemm R A and Kadowaki K 2015 *Appl. Phys. Lett.* **106** 092601
[33] Kashiwagi T, Sakamoto K, Kubo H, Shibano Y, Enomoto T, Kitamura T, Asanuma K, Yasui T, Watanabe C, Nakade K, Saiwai Y, Katsuragawa T, Tsujimoto M, Yoshizaki R, Yamamoto T, Minami H, Klemm R A and Kadowaki K 2015 *Appl. Phys. Lett.* **107** 082601
[34] Hao L Y, Ji M, Yuan J, An D Y, Li M Y, Zhou X J, Huang Y, Sun H C, Zhu Q, Rudau F, Wieland R, Kinev N, Li J, Xu W W, Jin B B, Chen J, Hatano T, Koshelets V P, Koelle D, Kleiner R, Wang H B and Wu P H 2015 *Phys. Rev. Applied* **3** 024006
[35] Minami H, Tsujimoto M, Kashiwagi T, Yamamoto T and Kadowaki K 2012 *IEICE T. Electron.* **E95-C** 347
[36] Minami H, Kakeya I, Yamaguchi H, Yamamoto T and Kadowaki K 2009 *Appl. Phys. Lett.* **95** 232511
[37] Li M Y, Yuan J, Kinev N, Li J, Gross B, Guénon S, Ishii A, Hirata K, Hatano T, Koelle D, Kleiner R, Koshelets V P, Wang H B and Wu P H 2012 *Phys. Rev. B* **86** 060505(R)
[38] Darula M, Doderer T and Beuven S 1999 *Supercond. Sci. Technol.* **12** R1
[39] Orita N, Minami H, Koike T, Yamamoto T and Kadowaki K 2010 *Physica C* **470** S786